

# Temporal changes of event size distribution during episodes of shallow tectonic tremor, Nankai trough

Masaru Nakano<sup>1</sup> and Suguru Yabe<sup>2</sup>

<sup>1</sup>Japan Agency for Marine-Earth Science and Technology

<sup>2</sup>Geological Survey of Japan, National Institute of Advanced Industrial Science and Technology (AIST)

November 24, 2022

## Abstract

Slow earthquakes follow a power-law size distribution with an exponential taper for the largest events. We investigated changes in the size distribution of shallow tectonic tremor events during two prolonged tremor episodes (>1 month) along the Nankai trough and found that the slope of the size distributions increased while the cut-off magnitudes decreased late during each episode, as tremor activity waned. Interpreting these changes with the two-dimensional probabilistic cell automaton model of slow earthquakes, we found that a decrease in event ignition probability or an increase in energy dissipation during slip can qualitatively explain the observed changes. These changes imply that a decrease in accumulated stress or pore-fluid pressure on the fault interface occurred during each tremor episode. Because the tremor source migrates during an episode, the changes in the size distribution parameters can be attributed to spatial variations or temporal changes in the source characteristics.

## Hosted file

20tremor-pca.v3.2.supplement.docx available at <https://authorea.com/users/539728/articles/603432-temporal-changes-of-event-size-distribution-during-episodes-of-shallow-tectonic-tremor-nankai-trough>



## 20 **Abstract**

21 Slow earthquakes follow a power-law size distribution with an exponential taper for the largest  
22 events. We investigated changes in the size distribution of shallow tectonic tremor events during  
23 two prolonged tremor episodes (>1 month) along the Nankai trough and found that the slope of  
24 the size distributions increased while the cut-off magnitudes decreased late during each episode,  
25 as tremor activity waned. Interpreting these changes with the two-dimensional probabilistic cell  
26 automaton model of slow earthquakes, we found that a decrease in event ignition probability or  
27 an increase in energy dissipation during slip can qualitatively explain the observed changes.  
28 These changes imply that a decrease in accumulated stress or pore-fluid pressure on the fault  
29 interface occurred during each tremor episode. Because the tremor source migrates during an  
30 episode, the changes in the size distribution parameters can be attributed to spatial variations or  
31 temporal changes in the source characteristics.

## 32 **Plain Language Summary**

33 The size distribution of slow earthquakes mostly follows a power law like that of ordinary  
34 earthquakes, in which the logarithm of event numbers is negatively proportional to the logarithm  
35 of event sizes, with an exponential taper for events larger than a cut-off magnitude. We  
36 investigated the changes in this size distribution during two prolonged episodes of shallow  
37 tectonic tremor that occurred on the plate interface along the Nankai trough, southwestern Japan.  
38 We found that the ratio of smaller events increased and the cut-off magnitude decreased as  
39 tremor activity decreased late in each episode. We interpreted this observation by using a model  
40 of slow earthquakes that divides a source fault into small cells and updates slip on each cell  
41 probabilistically. The model can explain the changes in the tremor size distribution by a decrease  
42 in the probability of event ignition or an increase in the energy dissipation during fault slip. This  
43 result implies that the accumulated stress or the pore-fluid pressure on the source fault decreased  
44 when the tremor was less active. Because the tremor source migrates during the course of each  
45 episode, these changes indicate that the source characteristics of tremor vary at different times or  
46 locations.

## 47 **1 Introduction**

48 Slow earthquakes, fault slips with longer durations than ordinary earthquakes of similar  
49 magnitudes, mostly occur in areas surrounding the source regions of megathrust earthquakes in  
50 subduction zones (e.g., Obara & Kato, 2016). Signals of a slow earthquake may be termed as  
51 tectonic tremor, a very low frequency earthquake (VLFE), or a slow slip event (SSE) depending  
52 on the frequency band of the observations, all of which share common fault slips because they  
53 occur concurrently in the same source region (e.g., Araki et al., 2017; Ito et al., 2007; Kaneko et  
54 al., 2018; Obara & Hirose, 2006; Obara et al., 2004; Rogers & Dragert, 2003). The source  
55 process of slow earthquakes is studied through the analysis of scaling relationships among the  
56 source characteristics: event duration, recurrence interval, size of the source fault, seismic  
57 moment release, radiated seismic energy, and so on (e.g., Ide & Yabe, 2014; Ide et al., 2007; Tan  
58 & Marson, 2020; Yabe et al., 2019). Recent studies suggest that heterogeneities in the frictional  
59 properties on the fault control the distribution of events and their source characteristics (e.g.,  
60 Baba et al., 2020; Nishikawa et al., 2019; Obara et al., 2010; Takemura et al., 2019; Tanaka et  
61 al., 2019).

62 The event size distribution is one of the scaling relationships that characterize the source  
 63 processes of seismic phenomena. Ordinary earthquakes follow the Ishimoto-Iida or Gutenberg-  
 64 Richter (GR) law (e.g., Gutenberg & Richter, 1944; Ishimoto & Iida, 1939), a power-law  
 65 relationship implying that the source fault is self-similar. The negative of the slope (the  $b$ -value)  
 66 is commonly related to the stress state of the medium (Scholz, 1968, 2015). In contrast, volcanic  
 67 tremor follow exponential-law size distributions (e.g., Benoit & McNutt, 2003), implying that  
 68 the source process has a characteristic size. Most studies have shown that slow earthquakes  
 69 follow a power-law size distribution (Bostock et al., 2015; Ito et al., 2009; Kao et al., 2010;  
 70 Nakamura & Sunagawa, 2015; Staudenmaier et al., 2019; Wech et al., 2010), although some  
 71 observations indicate that they follow an exponential-law size distribution (Chestler & Creager,  
 72 2017; Yabe & Ide, 2014).

73 A recent study of shallow tectonic tremor along the Nankai trough (Nakano et al., 2019)  
 74 found that the event size distribution follows a tapered Gutenberg-Richter (TGR) distribution  
 75 (Kagan, 2002), given by

$$76 \quad \Phi(M) = (M_t/M)^\beta \exp\left(\frac{M_t-M}{M_c}\right) \quad \text{for } M_t < M < \infty, \quad (1)$$

77 where  $M$  is seismic moment,  $M_t$  is the catalog completeness threshold, and  $M_c$  is the  
 78 corner moment.  $\beta$  controls the slope of the distribution;  $\beta = 2b/3$  in the ordinary Gutenberg-  
 79 Richter law. A TGR distribution may reconcile the contradictory findings of previous studies:  
 80 power-law distributions better fit the overall size distribution, but exponential distributions may  
 81 better fit the observations when only the largest events are observable. For ordinary earthquakes,  
 82 the  $b$ -value of the GR law, and accordingly  $\beta$ , has been related to the stress level in the medium  
 83 (Scholz, 1968, 2015), and the corner moment  $M_c$  may be related to the fault dimension, which is  
 84 specific to the causative fault (Kagan, 2002). For Nankai trough slow earthquakes, both  $\beta$  and  $M_c$   
 85 differ during different time periods in the same source region (Nakano et al., 2019), implying  
 86 that the source characteristics of these events change with time, although the cause is poorly  
 87 understood.

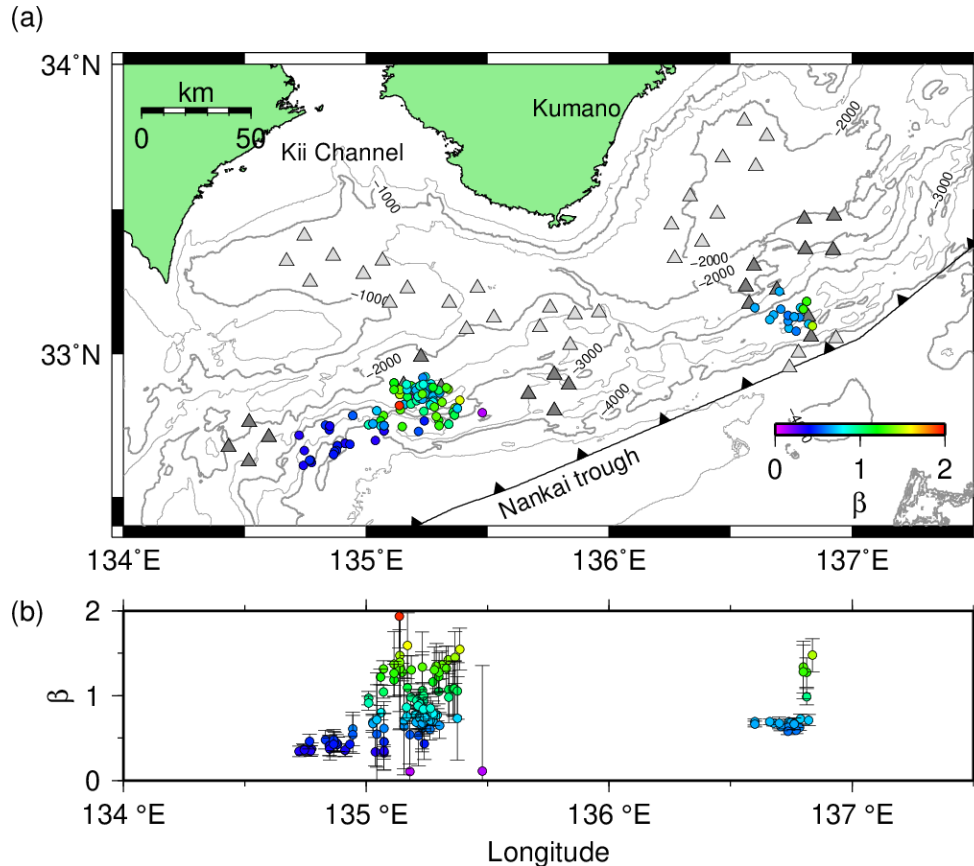
88 In this study, we analyzed the size distributions of shallow tectonic tremor along the  
 89 Nankai trough during tremor episodes that occurred off the city of Kumano, Mie Prefecture, in  
 90 2016 and off the Kii Channel in 2018. By fitting the data with the TGR distribution, we found  
 91 that the size distribution parameters of shallow tectonic tremor changed during the course of each  
 92 episode, indicating that the source characteristics changed. We qualitatively interpreted the  
 93 controlling factors of this distribution using the probabilistic cell automaton (PCA) model for  
 94 slow earthquakes proposed by Ide and Yabe (2019). We found that the changes in the tremor  
 95 event size distributions can be attributed to changes in the accumulated stress or the pore  
 96 pressure on the fault.

## 97 **2 Observed changes of tremor size distributions**

### 98 **2.1 Estimation of tremor size distribution**

99 Using data obtained from the permanent Dense Oceanfloor Network System for  
 100 Earthquakes and Tsunamis (DONET; Kaneda et al., 2015; Kawaguchi et al., 2015; Figure 1), we  
 101 analyzed intensive tremor episodes with durations longer than a month; these include one that  
 102 occurred off Kumano in April 2016, with a duration of about a month, and another off the Kii

103 Channel that started in mid-February 2018 and continued for about 4 months (Figure 1). We  
 104 referred to the seismic energy catalog of Nakano et al. (2019) for the 2016 off-Kumano activity,  
 105 and for this study we estimated the radiated seismic energy of tremor events during the 2018 off-  
 106 Kii Channel activity.



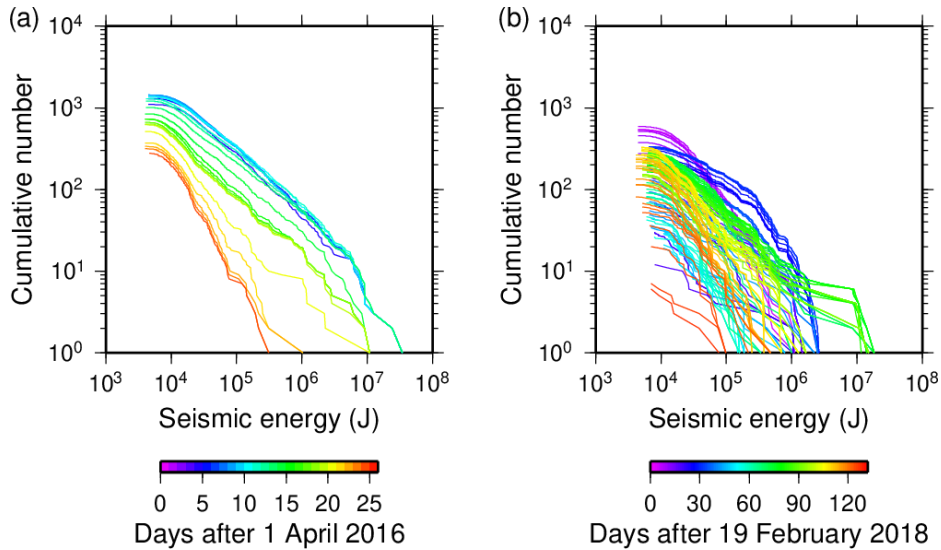
107

108 **Figure 1.** (a) Map showing locations of DONET stations (triangles) and 10-day average  
 109 locations of tectonic tremor events (circles). Dark gray triangles indicate DONET stations used  
 110 in this study. Colors of circles represent the slope ( $\beta$ ) of the size distribution of tremor events  
 111 (10-day averages). (b) Longitudinal distribution of  $\beta$ . Error bars indicate the standard error of  $\beta$   
 112 values.

113 We estimated tremor energy by the method of Nakano et al. (2019). We first determined  
 114 tremor source locations by the envelope correlation method (Ide, 2010; Obara, 2002). We used  
 115 the daily average of these locations (Figure S1) for energy estimations because of their large  
 116 scatter, which may be due to strong heterogeneities in velocity structures in the accretionary  
 117 prism (Takemura et al., 2020). We next computed the energy rate waveforms at the source from  
 118 three-component seismograms that were band-pass filtered between 2 and 8 Hz and corrected for  
 119 the site amplification factors given by Yabe et al. (2020). We defined a tremor event as one in  
 120 which the seismic energy rate continuously exceeded a threshold of  $10^2$  J/s. Nakano et al. (2019)  
 121 tried thresholds ranging between  $10$  and  $10^3$  J/s and found that they do not affect the nature of the  
 122 size distributions. The seismic energy of each tremor event was then obtained by integrating the  
 123 energy rate waveform over the time during each event. As the seismic energy of the tremor

124 signal is proportional to the seismic moment (Ide & Yabe, 2014; Yabe et al., 2019), we used  
 125 these seismic energy estimates to represent the tremor event size. Signals from ordinary  
 126 earthquakes were removed by reference to the catalogs of the Japan Meteorological Agency and  
 127 U.S. Geological Survey.

128 To investigate the changes in event size distributions during each tremor episode, we  
 129 fitted the TGR distribution given by equation (1) to the size distributions obtained from sliding  
 130 10-day time windows (Figure 2). We assumed a catalog completeness magnitude  $M_t$  of  $3.0 \times 10^4$   
 131 J.



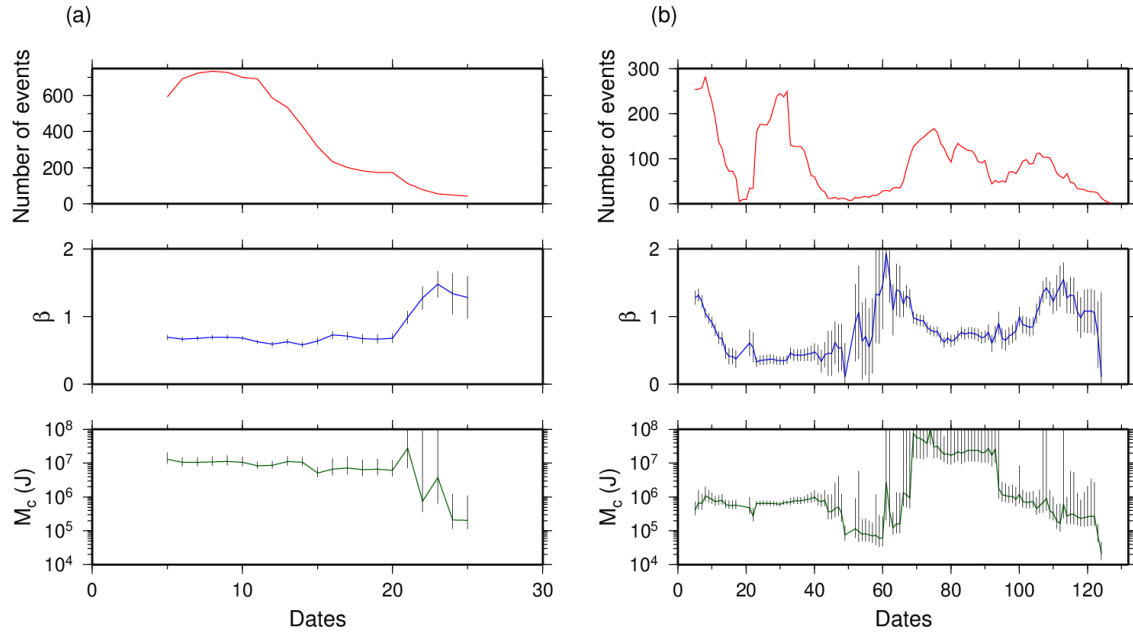
132

133 **Figure 2.** Size distributions of tectonic tremor during successive 10-day sliding time windows  
 134 for (a) the 2016 off-Kumano episode and (b) the 2018 off-Kii Channel episode.

135

## 2.2 Changes of tremor size distributions

136 Figure 3 shows how the size-distribution parameters  $\beta$  and  $M_c$  of the TGR distribution  
 137 changed with time for the 2016 off-Kumano and 2018 off-Kii Channel tremor episodes;  $\beta$   
 138 increased and  $M_c$  decreased near the end of the 2016 episode and in the middle and end of the  
 139 2018 episode. The change was also clear in the event size distributions of successive 10-day time  
 140 windows (Figure 2). Because the tremor source migrated during each episode (Figure S1), we  
 141 plotted the distributions of  $\beta$  and  $M_c$  in Figures 1 and S2, respectively, at positions representing  
 142 the 10-day average of tremor source locations. In the 2016 off-Kumano episode, higher  $\beta$  values  
 143 with lower  $M_c$  were concentrated at the southeast end of the source area. In the 2018 off-Kii  
 144 Channel episode, the activity was mainly concentrated between longitude  $135.0^\circ\text{E}$  and  $135.5^\circ\text{E}$ ,  
 145 and both  $\beta$  and  $M_c$  showed distinct variations in this area. We note that these estimations were  
 146 from tremor events scattered within 10–20 km of the average location. These results imply that  
 147 the changes in the size-distribution parameters may be caused by spatial or temporal changes in  
 148 the source characteristics of the tremor events.



149

150 **Figure 3.** Temporal changes of event number and the slope  $\beta$  and corner moment  $M_c$  of the  
 151 tremor size distributions obtained from 10-day sliding time windows during the (a) 2016 off-  
 152 Kumano and (b) 2018 off-Kii Channel episodes. Vertical bars represent uncertainties on  $\beta$  and  
 153  $M_c$ .

### 154 3 Size distribution of slow earthquakes expected from the 2D PCA model

#### 155 3.1 2D PCA model

156 We investigated the cause of the observed changes in the tremor event size distributions  
 157 by using the 2D PCA model of slow earthquakes proposed by Ide and Yabe (2019), which is an  
 158 extension of the 1D Brownian slow earthquake model (Ide, 2008) to a 2D source fault. This  
 159 model has successfully reproduced various scaling relationships of slow earthquakes, including  
 160 their TGR-like event size distributions. In the 2D PCA model, the fault plane of a slow  
 161 earthquake is divided into  $N_x \times N_y$  cells, and each cell has two states: “stop” and “slip”. The  
 162 state of each cell is updated stochastically according to the states of neighboring cells: Each  
 163 “stop” cell becomes a “slip” cell with a probability  $N_b p_b$ , where  $N_b$  is the number of surrounding  
 164 cells in the “slip” state and  $p_b$  is a probability of interactions between adjacent cells, and each  
 165 “slip” cell becomes a “stop” cell with a probability  $(4 - N_b)p_b$ . In addition, Ide & Yabe (2019)  
 166 introduced the random ignition of slip in a cell with a probability  $p_l$ , which may be related to the  
 167 slow loading from the surrounding medium. They also considered energy dissipation during slip,  
 168 which suppresses slip in the cell with a probability  $p_v$ , introducing an additional characteristic  
 169 scale to the event size distribution. The status of each cell ( $v_i^k$ ) is updated based on

$$170 \quad v_i^{k+1} = H(v_i^k + p_b \sum_{NN} (v_j^k - v_i^k) + p_l - p_v v_i^k - \xi), \quad (2)$$

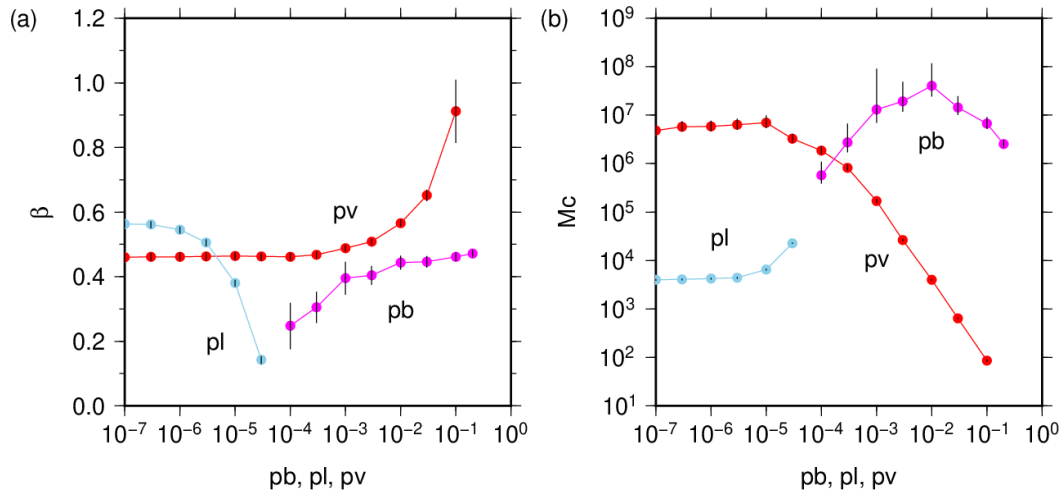
171 where  $NN$  represents the four nearest neighbor cells,  $H()$  is the Heaviside function,  $i$  and  
 172  $k$  represent the cell number and time step, respectively, and  $\xi$  is a random number with a

173 uniform distribution between 0 and 1 (Ide & Yabe, 2019). The value of  $v_i^k$  is 0 in the “stop” state  
 174 and 1 in the “slip” state.

### 175 3.2 Dependence of tremor size distribution on probability parameters

176 We used the 2D PCA model to investigate the dependence of  $\beta$  and  $M_c$  for the tremor  
 177 size distribution on each of the probability parameters for synthetic tremor. We simulated tremor  
 178 events with a fixed source size  $N_x = N_y = 101$  for  $10^6$  steps. The tremor event size was defined  
 179 as the total number of slipped cells during a tremor event, which ends when the number of  
 180 slipping cells becomes zero. The dependence on  $p_b$  was surveyed for tremor events computed  
 181 with  $p_l = p_v = 0.0$ . The dependences on  $p_v$  and  $p_l$  were studied for fixed values of  $p_l = 0.0$  and  
 182  $p_v = 0.01$ , respectively, with  $p_b = 0.1$ . We note here that  $p_l$  should be smaller than  $p_v$ ,  
 183 otherwise the slipping cells proliferate without suppression (see equation 2). Then we estimated  
 184 the size-distribution parameters  $\beta$  and  $M_c$  by fitting the TGR distribution to the event size  
 185 distributions synthesized by using each combination of the probability parameters by setting  
 186  $M_t = 100$  event size units. The event size distributions of the synthetic tremor computed by  
 187 varying  $p_b$ ,  $p_l$ , and  $p_v$  are shown in Figures S3, S4, and S5, respectively.

188 Figure 4 shows the dependence of  $\beta$  and  $M_c$  values for each probability parameter of the  
 189 2D PCA model. When the ignition probability  $p_l$  increases, the slope  $\beta$  of the size distribution  
 190 decreases while the corner event size  $M_c$  increases. The anti-correlation of  $p_l$  and  $\beta$  is similar to  
 191 the known anti-correlation between the  $b$ -value of the GR law and the stress level in the medium  
 192 for regular earthquakes (Scholz, 1968, 2015). The dependence on the stopping probability  $p_v$   
 193 was opposite to the dependence on  $p_l$ . This behavior is easily understood because these  
 194 probability parameters have opposite signs in equation (2). Energy dissipation during slip  
 195 suppresses growth of the event, and accordingly the ratio of large events to small events  
 196 decreases. This effect introduces an additional characteristic size to the system and accordingly  
 197 reduces  $M_c$ . The dependence on the probability  $p_b$  is rather complex. Both  $\beta$  and  $M_c$  increase as  
 198  $p_b$  increases for  $p_b < 10^{-2}$ , whereas  $M_c$  decreases while  $\beta$  remains almost constant for  $p_b >$   
 199  $10^{-2}$ . When  $p_b$  is too small, slip on a cell hardly propagates to surrounding cells and a slipping  
 200 cell hardly stops, in which case the event size is mostly determined by the duration of slip at one  
 201 cell. We do not expect such behavior for the source of short-term slow earthquake episodes.  
 202 When  $p_b$  is large enough, slip on a cell easily propagates to surrounding cells and slip in a cell  
 203 easily stops when it is surrounded by “stop” cells, which may reduce event durations and  
 204 decrease  $M_c$  at the largest  $p_b$  values.



205

206 **Figure 4.** Dependence of the size distribution parameters  $\beta$  and  $M_c$  of synthetic tremor activities  
 207 on three probability parameters ( $p_b$ ,  $p_l$ , and  $p_v$ ) computed from the 2D PCA model (Ide & Yabe,  
 208 2019). See section 3 in the text for explanation.

#### 209 4 Discussion

210 In both of the tremor episodes we studied along the Nankai trough,  $\beta$  increased as  $M_c$   
 211 decreased in the later part of the episode as the rate of events decreased. These changes can be  
 212 qualitatively explained in the 2D PCA model by a decrease in the event ignition probability  $p_l$  or  
 213 an increase in the energy dissipation probability  $p_v$ . In the following, we discuss the causes that  
 214 may change these probabilistic parameters during slow earthquakes. Because the tremor sources  
 215 migrated during each episode (Figure S1), the changes in these parameters may represent spatial  
 216 or temporal changes in the source characteristics.

217 The main factors that control slow earthquake activity are the stiffness of the host rock,  
 218 stress accumulation, and frictional resistance on the fault interface. Host rock stiffness may  
 219 control the interactions of fault slip with the local surroundings, which was modeled as the  
 220 probability  $p_b$  in the 2D PCA model, but cannot explain the observed changes of the tremor size  
 221 distributions.

222 Accumulated stress on the causative fault drives the spontaneous activity of regular and  
 223 slow earthquakes (e.g., Matsuzawa et al., 2010). Accumulated stress that is initially high is  
 224 released gradually in slow earthquakes. This change may decrease the event ignition probability  
 225  $p_l$  that is consistent with the observed  $\beta$  increase and  $M_c$  decrease in the later part of tremor  
 226 episodes. Because the slip history of previous slow earthquakes may result in a heterogeneous  
 227 distribution of accumulated stress (e.g., Matsuzawa et al., 2010), the migration of tremor sources  
 228 may also affect the tremor size distributions. It is challenging to estimate the stress accumulation  
 229 on a source fault before an event occurs; however, the degree of coupling between the overriding  
 230 and subducting plate may affect the stress accumulation rate and accordingly the slip ignition  
 231 probability. The coupling ratio on the plate interface has been found to be spatially  
 232 heterogeneous along the Nankai trough (Nishimura et al., 2018; Noda et al., 2018; Yokota et al.,  
 233 2016) and is inversely correlated with slow earthquake activity (Baba et al., 2020; Takemura et

234 al., 2019). Hence, spatial variations of the coupling ratio may also be related to event size  
235 distributions.

236 Frictional resistance depends on the pore-fluid pressure on the fault interface. Because an  
237 increase in pore-fluid pressure reduces the normal stress and accordingly the frictional resistance,  
238 pore fluid is considered a primary trigger of slow earthquakes (e.g., Kato et al., 2010; Obara,  
239 2002). Theoretical studies modeling slow earthquakes have assumed that pore fluid reduces the  
240 normal stress on the fault (e.g., Gao & Wang, 2017; Liu & Rice, 2007; Matsuzawa et al., 2010).  
241 A decrease in pore-fluid pressure increases frictional resistance during slip and therefore  
242 increases the energy dissipation probability  $p_v$  or decreases the slip ignition probability  $p_l$  in the  
243 2D PCA model. The observed  $\beta$  increase and  $M_c$  decrease can be explained by a decrease of  
244 pore-fluid pressure as tremor activity decreases in the later part of tremor episodes.

245 The excess pore-fluid pressure inferred from low shear-wave velocity anomalies in the  
246 accretionary prism has been correlated with the distribution of shallow VLFs along the Nankai  
247 trough (Kitajima & Saffer, 2012; Tonegawa et al., 2017). Recent studies have detected along-dip  
248 and along-strike variations of tremor and VLF activities, implying that heterogeneous frictional  
249 properties on the plate interface affect slow earthquake activity (Nishikawa et al., 2019; Tanaka  
250 et al., 2019; Yabe et al., 2019, 2020). The heterogeneous distribution of pore-fluid pressure and  
251 frictional properties on the fault interface may change the event size distribution of tremor as it  
252 migrates. At shallow depths, the frictional properties of clay gouge produce velocity-  
253 strengthening behavior when water is included in minerals' interlayers (Ikari et al., 2007). Clay  
254 minerals become dehydrated at depths greater than 8 km by the increased temperature and  
255 pressure, and the resulting fluid may exist in pore spaces rather than in the clay minerals (Ikari et  
256 al., 2007). The dehydration depth is close to the source depths of VLFs along the Nankai trough  
257 (Nakano et al., 2018; Sugioka et al., 2012). Since VLFs and tectonic tremor are the same  
258 phenomena but observed in different frequency ranges (Kaneko et al., 2018; Masuda et al.,  
259 2020), depth-dependent frictional properties may also affect the event size distribution of  
260 tectonic tremor.

261 Seismic observations have detected migrations of pore fluid coincident with slow  
262 earthquakes (Gosselin et al., 2020; Kano et al., 2019; Nakajima & Uchida, 2018; Warren-Smith  
263 et al., 2019; Zal et al., 2020), implying that pore-fluid pressure on the fault changes during a  
264 tremor episode. Tidal stress changes also affect normal stress and thereby tremor activity (e.g.,  
265 Ide & Tanaka, 2014), but we can ignore this effect because the changes we detected in size  
266 distribution parameters occurred in time windows 10 days long.

267 In this study, we interpreted observed changes in the size distributions of tectonic tremor  
268 based on the 2D PCA model. The slope  $\beta$  expected from the 2D PCA model is usually 0.5, a  
269 value that is smaller than the observed values except for the largest  $p_v$  values. Although the 2D  
270 PCA model reproduces certain statistical characteristics of slow earthquakes, such as duration-  
271 moment scaling and TGR size distribution, there remains room for improvement. For example,  
272 the 2D PCA model only considers interactions with the nearest neighboring cells and ignores  
273 interactions with more distant cells. It also does not include the effects of slip history, which are  
274 necessary to reproduce lateral migrations over long distances. Therefore, the interpretations in  
275 this study are still qualitative. Further improvement of data analysis and theoretical models is  
276 needed to improve our understanding of the source process of slow earthquakes.

277 **5 Conclusions**

278 Shallow tectonic tremor along the Nankai trough follow the tapered Gutenberg-Richter  
279 distribution (Kagan, 2002), a power-law distribution of event sizes with an exponential taper for  
280 the largest events. In our study of temporal changes of the event size distribution of shallow  
281 tectonic tremor during long tremor episodes off Kumano in 2016 and off the Kii Channel in  
282 2018, we found that the slope of the event size distribution increased while the cut-off magnitude  
283 decreased in the later part of each episode. The 2D PCA model of slow earthquakes (Ide & Yabe,  
284 2019) allowed us to interpret the observed changes in the tremor size distribution qualitatively by  
285 a decrease in the probability of slip ignition on the fault or an increase in energy dissipation  
286 during slip. These changes can be attributed to the release of accumulated stress by slow  
287 earthquakes or spatial-temporal variations of pore-fluid pressures during slow earthquakes.

288 **Acknowledgments, Samples, and Data**

289 This study was supported by KAKENHI Grants JP16H06477 (to M. N.), JP19K04050 (to  
290 M. N.), and JP18K13639 (to S. Y.) from the Japan Society for the Promotion of Science. All  
291 figures were drawn with Generic Mapping Tools (Wessel & Smith, 1998). Seismic waveform  
292 data from DONET can be downloaded from <http://www.hinet.bosai.go.jp/?LANG=en> (National  
293 Research Institute for Earth Science and Disaster Resilience, 2019). The earthquake catalog of  
294 the Japan Meteorological Agency can be downloaded from  
295 <http://www.data.jma.go.jp/svd/eqev/data/bulletin/hypo.html>. The earthquake catalog of the  
296 United States Geological Survey can be downloaded from  
297 <https://earthquake.usgs.gov/earthquakes/search/>.

299 **References**

- 300 Araki, E., Saffer, D.M., Kopf, A.J., Wallace, L.M., Kimura, T., Machida, Y., Ide, S., Davis, E.,  
301 & IODP Expedition 365 shipboard scientists (2017). Recurring and triggered slow-slip  
302 events near the trench at the Nankai Trough subduction megathrust. *Science*, 356 (6343),  
303 1157-1160. <http://doi.org/10.1126/science.aan3120>
- 304 Baba, S., Takemura, S., Obara, K., & Noda, A. (2020). Slow earthquakes illuminating interplate  
305 coupling heterogeneities in subduction zones. *Geophysical Research Letters*, 47,  
306 e2020GL088089. <https://doi.org/10.1029/2020GL088089>
- 307 Benoit, J., & McNutt, S. (2003). Duration-amplitude distribution of volcanic tremor. *Journal of*  
308 *Geophysical Research*, 108, 2146. <https://doi.org/10.1029/2001JB001520>
- 309 Bostock, M. G., Thomas, A. M., Savard, G., Chuang, L., & Rubin, A. M. (2015). Magnitudes  
310 and moment-duration scaling of low-frequency earthquakes beneath southern Vancouver  
311 Island. *Journal of Geophysical Research: Solid Earth*, 120, 6329–6350.  
312 <https://doi.org/10.1002/2015JB012195>
- 313 Chestler, S. R., & Creager K. C. (2017). Evidence for a scale-limited low-frequency earthquake  
314 source process. *Journal of Geophysical Research: Solid Earth*, 122, 3099–3114,  
315 <https://doi.org/10.1002/2016JB013717>
- 316 Gao, X., & Wang, K. (2017). Rheological separation of the megathrust seismogenic zone and  
317 episodic tremor and slip, *Nature*, 543, 416–419, <https://doi.org/10.1038/nature21389>

- 318 Gosselin, J. M., Audet, P., Estève, C., McLellan, M., Mosher, S. G., & Schaeffer, A. J., (2020).  
319 Seismic evidence for megathrust fault-valve behavior during episodic tremor and slip,  
320 *Science Advances*, 6, eaay5174, <https://doi.org/10.1126/sciadv.aay5174>
- 321 Gutenberg, B., & Richter, C. F. (1944). Frequency of earthquakes in California. *Bulletin of*  
322 *Seismological Society of America*, 34, 185–188.
- 323 Ide, S. (2008). A Brownian walk model for slow earthquakes. *Geophysical Research Letters*, 35,  
324 L17301, <https://doi.org/10.1029/2008GL034821>
- 325 Ide, S. (2010). Striations, duration, migration and tidal response in deep tremor. *Nature*, 466,  
326 356–359, <https://doi.org/10.1038/nature09251>
- 327 Ide, S., Beroza, G. C., Shelly, D. R., & Uchide, T. (2007). A scaling law for slow earthquakes,  
328 *Nature*, 447, 76–79, <https://doi.org/10.1038/nature05780>
- 329 Ide, S., & Tanaka, Y. (2014). Controls on plate motion by oscillating tidal stress: Evidence from  
330 deep tremors in western Japan, *Geophysical Research Letters*, 41, 3842–3850,  
331 <https://doi.org/10.1002/2014GL060035>
- 332 Ide, S., & Yabe, S. (2014). Universality of slow earthquakes in the very low frequency band,  
333 *Geophysical Research Letters*, 41, 2786–2793.  
334 <https://doi.org/doi:10.1002/2014GL059712>
- 335 Ide, S., & Yabe, S. (2019). Two-Dimensional Probabilistic Cell Automaton Model for  
336 Broadband Slow Earthquakes. *Pure and Applied Geophysics*, 176, 1021–1036,  
337 <https://doi.org/10.1007/s00024-018-1976-9>
- 338 Ikari, M. J., Saffer, D. M., & Marone, C. (2007). Effect of hydration state on the frictional  
339 properties of montmorillonite-based fault gouge, *Journal of Geophysical Research: Solid*  
340 *Earth*, 112, B06423, <https://doi.org/10.1029/2006JB004748>
- 341 Ishimoto, M., & Iida, K. (1939). Observations of earthquakes registered with the  
342 microseismograph constructed recently. *Bulletin of Earthquake Research Institute*  
343 *University of Tokyo*, 17, 443–478.
- 344 Ito, Y., Obara, K., Shiomi, K., Sekine, S., & Hirose, H. (2007). Slow Earthquakes Coincident  
345 with Episodic Tremors and Slow Slip Events. *Science*, 315, 503-506.  
346 <https://doi.org/10.1126/science.1134454>
- 347 Ito, Y., Obara, K., Matsuzawa, T., & Maeda, T. (2009). Very low frequency earthquakes related  
348 to small asperities on the plate boundary interface at the locked to aseismic transition,  
349 *Journal of Geophysical Research: Solid Earth*, 114, B00A13.  
350 <https://doi.org/10.1029/2008JB006036>
- 351 Kagan, Y. Y. (2002). Seismic moment distribution revisited: I. Statistical results. *Geophysical*  
352 *Journal International*, 148, 520–541.
- 353 Kaneda, Y., Kawaguchi, K., Araki, E., Matsumoto, H., Nakamura, T., Kamiya, S., Ariyoshi, K.,  
354 Hori, T., Baba, T., & Takahashi, N. (2015). Development and application of an advanced  
355 ocean floor network system for megathrust earthquakes and tsunamis. In Favali P et al.  
356 (eds) *Seafloor Observatories*. Springer, Heidelberg, pp 643–662.  
357 [https://doi.org/10.1007/978-3-642-11374-1\\_252](https://doi.org/10.1007/978-3-642-11374-1_252)

- 358 Kaneko, L., Ide, S., & Nakano, M. (2018). Slow earthquakes in the microseism frequency band  
359 (0.1–1.0 Hz) off Kii Peninsula, Japan. *Geophysical Research Letters*, 45, 2618–2624.  
360 <https://doi.org/10.1002/2017GL076773>
- 361 Kano, M., Kato, A., & Obara, K. (2019). Episodic tremor and slip silently invades strongly  
362 locked megathrust in the Nankai Trough, *Scientific Reports*, 9, 9270.  
363 <https://doi.org/10.1038/s41598-019-45781-0>
- 364 Kao, H., Wang, K., Dragert, H., Kao, J. Y., & Rogers, G. (2010). Estimating seismic moment  
365 magnitude (M<sub>w</sub>) of tremor bursts in northern Cascadia: Implications for the “seismic  
366 efficiency” of episodic tremor and slip. *Geophysical Research Letters*, 37, L19306.  
367 <https://doi.org/10.1029/2010GL044927>
- 368 Kato, A., Iidaka, T., Ikuta, R., Yoshida, Y., Katsumata, K., Iwasaki, T., Sakai, S., Thurber, C.,  
369 Tsumura, N., Yamaoka, K., Watanabe, T., Kunitomo, T., Yamazaki, F., Okubo, M.,  
370 Suzuki, S., & Hirata, N. (2010). Variations of fluid pressure within the subducting  
371 oceanic crust and slow earthquakes, *Geophysical Research Letters*, 37, L14310.  
372 <https://doi.org/doi:10.1029/2010GL043723>
- 373 Kawaguchi, K., Kaneko, S., Nishida, T., & Komine, T. (2015). Construction of the DONET real-  
374 time seafloor observatory for earthquakes and tsunami monitoring, In Favali P et al. (eds)  
375 Seafloor Observatories. Springer, Heidelberg, pp. 211–228. [https://doi.org/10.1007/978-](https://doi.org/10.1007/978-3-642-11374-1_10)  
376 [3-642-11374-1\\_10](https://doi.org/10.1007/978-3-642-11374-1_10)
- 377 Kitajima, H., & Saffer, D. M. (2012). Elevated pore pressure and anomalously low stress in  
378 regions of low frequency earthquakes along the Nankai Trough subduction megathrust,  
379 *Geophysical Research Letters*, 39, L23301. <https://doi.org/10.1029/2012GL053793>
- 380 Liu, Y., & Rice, J. R. (2007). Spontaneous and triggered aseismic deformation transients in a  
381 subduction fault model, *Journal of Geophysical Research*, 112, B09404.  
382 <https://doi.org/10.1029/2007JB004930>
- 383 Masuda, K., Ide, S., Ohta, K., & Matsuzawa, T. (2020). Bridging the gap between low-frequency  
384 and very-low-frequency earthquakes, *Earth Planets and Space*, 72:47.  
385 <https://doi.org/10.1186/s40623-020-01172-8>
- 386 Matsuzawa, T., Hirose, H., Shibasaki, B., & Obara, K. (2010). Modeling short- and long-term  
387 slow slip events in the seismic cycles of large subduction earthquakes, *Journal of*  
388 *Geophysical Research*, 115, B12301. <https://doi.org/10.1029/2010JB007566>
- 389 Nakajima, J., & Uchida, N. (2018). Repeated drainage from megathrusts during episodic slow  
390 slip, *Nature Geoscience*, 11, 351–356. <https://doi.org/10.1038/s41561-018-0090-z>
- 391 Nakamura, M., & Sunagawa, N. (2015). Activation of very low frequency earthquakes by slow  
392 slip events in the Ryukyu Trench. *Geophysical Research Letters*, 42, 1076–1082.  
393 <https://doi.org/10.1002/2014GL062929>
- 394 Nakano, M., Hori, T., Araki, E., Kodaira, S., & Ide, S. (2018). Shallow very-low-frequency  
395 earthquakes accompany slow slip events in the Nankai subduction zone. *Nature*  
396 *Communications*, 9, 984. <https://doi.org/10.1038/s41467-018-03431-5>

- 397 Nakano, M., Yabe, S., Sugioka, H., Shinohara, M., & Ide, S. (2019). Event size distribution of  
398 shallow tectonic tremor in the Nankai trough. *Geophysical Research Letters*, 46, 5828–  
399 5836. <https://doi.org/10.1029/2019GL083029>
- 400 National Research Institute for Earth Science and Disaster Resilience (2019), NIED DONET,  
401 National Research Institute for Earth Science and Disaster Resilience,  
402 <https://doi.org/10.17598/NIED.0008>
- 403 Nishikawa, T., Matsuzawa, T., Ohta, K., Uchida, N., Nishimura, T., & Ide, S. (2019). The slow  
404 earthquake spectrum in the Japan Trench illuminated by the S-net seafloor observatories.  
405 *Science* 365 (6455), 808–813. <https://doi.org/10.1126/science.aax5618>
- 406 Nishimura, T., Yokota, Y., Tadokoro, K., & Ochi, T. (2018). Strain partitioning and interplate  
407 coupling along the northern margin of the Philippine Sea plate, estimated from Global  
408 Navigation Satellite System and Global Positioning System-Acoustic data. *Geosphere*,  
409 14, 535–551. <https://doi.org/10.1130/GES01529.1>
- 410 Noda, A., Saito, T., & Fukuyama, E. (2018). Slip-deficit rate distribution along the Nankai  
411 trough, Southwest Japan, with elastic lithosphere and viscoelastic asthenosphere. *Journal*  
412 *of Geophysical Research*, 123, 8125–8142. <https://doi.org/10.1029/2018JB015515>
- 413 Obara, K. (2002). Nonvolcanic Deep Tremor Associated with Subduction in Southwest Japan.  
414 *Science*, 296, 1679–1681. <https://doi.org/10.1126/science.1070378>
- 415 Obara, K., Hirose, H., Yamamizu, F., & Kasahara, K. (2004). Episodic slow slip events  
416 accompanied by non-volcanic tremors in southwest Japan subduction zone, *Geophysical*  
417 *Research Letters*, 31, L23602. <https://doi.org/10.1029/2004GL020848>
- 418 Obara, K., & Hirose, H. (2006). Non-volcanic deep low-frequency tremors accompanying slow  
419 slips in the southwest Japan subduction zone, *Tectonophysics*, 417, 33–51.  
420 <https://doi.org/10.1016/j.tecto.2005.04.013>
- 421 Obara, K., Tanaka, S., Maeda, T., & Matsuzawa, T. (2010). Depth-dependent activity of non-  
422 volcanic tremor in southwest Japan, *Geophysical Research Letters*, 37, L13306.  
423 <https://doi.org/10.1029/2010GL043679>
- 424 Obara, K., & Kato, A. (2016). Connecting slow earthquakes to huge earthquakes. *Science*, 353,  
425 253–257. <https://doi.org/10.1126/science.aaf1512>
- 426 Rogers, T., & Dragert, H. (2003). Episodic tremor and slip on the Cascadia subduction zone: The  
427 chatter of silent slip, *Science*, 300 (5627), 1942–1943.  
428 <https://doi.org/10.1126/science.1084783>
- 429 Scholz, C. H. (1968). The frequency–magnitude relation of microfracturing in rock and its  
430 relation to earthquakes. *Bulletin of the Seismological Society of America*, 58, 399–415.
- 431 Scholz, C. H. (2015). On the stress dependence of the earthquake b value. *Geophysical Research*  
432 *Letters*, 42, 1399–1402. <https://doi.org/10.1002/2014GL062863>
- 433 Staudenmaier, N., Tormann, T., Edwards, B., Mignan, A., & Wiemer, S. (2019). The frequency-  
434 size scaling of non-volcanic tremors beneath the San Andreas Fault at Parkfield: Possible  
435 implications for seismic energy release, *Earth and Planetary Science Letters*, 516, 77–  
436 107. <https://doi.org/10.1016/j.epsl.2019.04.006>

- 437 Sugioka, H., Okamoto, T., Nakamura, T., Ishihara, Y., Ito, A., Obana, K., Kinoshita, M.,  
438 Nakahigashi, K., Shinohara, M., & Fukao, Y. (2012). Tsunamigenic potential of the  
439 shallow subduction plate boundary inferred from slow seismic slip. *Nature Geoscience*, 5,  
440 414–418. <https://doi.org/10.1038/NGEO1466>
- 441 Takemura, S., Noda, A., Kubota, T., Asano, Y., Matsuzawa, T., & Shiomi, K. (2019). Migrations  
442 and clusters of shallow very low frequency earthquakes in the regions surrounding shear  
443 stress accumulation peaks along the Nankai trough. *Geophysical Research Letters*, 46,  
444 11,830–11,840. <https://doi.org/10.1029/2019GL084666>
- 445 Takemura, S., Yabe, S., & Emoto, K., (2020). Modelling high-frequency seismograms at ocean  
446 bottom seismometers: effects of heterogeneous structures on source parameter estimation  
447 for small offshore earthquakes and shallow low-frequency tremors, *Geophysical Journal  
448 International*, 223, 1708–1723. <https://doi.org/10.1093/gji/ggaa404>
- 449 Tan, Y. J., & Marsan, D. (2020). Connecting a broad spectrum of transient slip on the San  
450 Andreas fault, *Science Advances*, 6, eabb2489. <https://doi.org/10.1126/sciadv.abb2489>
- 451 Tanaka, S., Matsuzawa, T., & Asano, Y. (2019). Shallow low–frequency tremor in the northern  
452 Japan Trench subduction zone. *Geophysical Research Letters*, 46, 5217–5224.  
453 <https://doi.org/10.1029/2019GL082817>
- 454 Tonegawa, T., Araki, E., Kimura, T., Nakamura, T., Nakano, M. & Suzuki, K. (2017). Sporadic  
455 low-velocity volumes spatially correlate with shallow very low frequency earthquake  
456 clusters. *Nature Communications*, 8, 2048. <https://doi.org/10.1038/s41467-017-02276-8>
- 457 Warren-Smith, E., Fry, B., Wallace, L., Chon, E., Henrys, S., Sheehan, A., Mochizuki, K.,  
458 Schwartz, S., Webb, S., & Lebedev, S. (2019). Episodic stress and fluid pressure cycling  
459 in subducting oceanic crust during slow slip. *Nature Geoscience*, 12, 475–481.  
460 <https://doi.org/10.1038/s41561-019-0367-x>
- 461 Wech, A. G., Creager, K. C., Houston, H., & Vidale, J. E. (2010). An earthquake-like  
462 magnitude-frequency distribution of slow slip in northern Cascadia. *Geophysical  
463 Research Letters*, 37, L22310. <https://doi.org/10.1029/2010GL044881>
- 464 Wessel, P., & Smith, W. H. F. (1998). New, improved version of generic mapping tools released.  
465 *Eos, Transactions American Geophysical Union*, 79(47), 579.  
466 <https://doi.org/10.1029/98EO00426>
- 467 Yabe, S., & Ide, S. (2014). Spatial distribution of seismic energy rate of tectonic tremors in  
468 subduction zones. *Journal of Geophysical Research: Solid Earth*, 119, 8171–8185.  
469 <https://doi.org/10.1002/2014JB011383>
- 470 Yabe, S., Tonegawa, T., & Nakano, M. (2019). Scaled energy estimation for shallow slow  
471 earthquakes. *Journal of Geophysical Research: Solid Earth*, 124, 1507–1519.  
472 <https://doi.org/10.1029/2018JB016815>
- 473 Yabe, S., Baba, S., Tonegawa, T., Nakano, M., & Takemura, S. (2020). Seismic energy radiation  
474 and along-strike heterogeneities of shallow tectonic tremors at the Nankai Trough and  
475 Japan Trench, *EarthArXiv*. <https://doi.org/10.31223/X57C71>

- 476 Yokota, Y., Ishikawa, T., Watanabe, S., Tashiro, T., & Asada, A. (2016). Seafloor geodetic  
477 constrains on interplate coupling of the Nankai Trough megathrust zone. *Nature*, 534,  
478 374–377. <https://doi.org/10.1038/nature17632>
- 479 Zal, H. J., Jacobs, K., Savage, M. K., Yarcec, J., Mroczek, S., Graham, K., Todd, E. K., Nakai,  
480 J., Iwasaki, Y., Sheehan, A., Mochizuki, K., Wallace, L., Schwartz, S., Webb, S., &  
481 Henrys, S. (2020). Temporal and spatial variations in seismic anisotropy and  $V_P/V_S$  ratios  
482 in a region of slow slip. *Earth and Planetary Science Letters*, 532, 115970.  
483 <https://doi.org/10.1016/j.epsl.2019.115970>